Journal of Advanced Ceramics
2017, **6**(4): 351–359
https://doi.org/10.1007/s40145-017-0247-z

ISSN 2226-4108
CN 10-1154/TQ

Research Article

Synthesis of Al_4SiC_4 powders via carbothermic reduction: Reaction and grain growth mechanisms

Xinming XING[a], Junhong CHEN[a,*], Guoping BEI[b], Bin LI[c], Kuo-Chih CHOU[c], Xinmei HOU[c,*]

[a]*School of Material Science and Technology*, *University of Science and Technology Beijing*, *Beijing 100083*, *China*
[b]*Department of Materials Science and Engineering*, *3ME*, *Delft University of Technology*, *Delft*, *2628CD*, *the Netherlands*
[c]*State Key Laboratory of Advanced Metallurgy*, *University of Science and Technology Beijing*, *Beijing 100083*, *China*

Received: July 08, 2017; Revised: August 22, 2017; Accepted: September 08, 2017

Abstract: Highly pure Al_4SiC_4 powders were prepared by carbothermic reduction at 2173 K using Al_2O_3, SiO_2, and graphite as raw materials. The obtained Al_4SiC_4 powders owned hexagonal plate-like grains with a diameter of about 200–300 μm and a thickness of about 2–6 μm. Based on the experimental results, the reaction of Al_4SiC_4 formation and grain evolution mechanisms were determined from thermodynamic and first-principles calculations. The results indicated that the synthesis of Al_4SiC_4 by the carbothermic reduction consisted of two parts, i.e., solid–solid reactions initially followed by complex gas–solid and gas–gas reactions. The grain growth mechanism of Al_4SiC_4 featured a two-dimensional nucleation and growth mechanism. The gas phases formed during the sintering process favored the preferential grain growth of (0010) and $(1\bar{1}0)$ planes resulting in formation of hexagonal plate-like Al_4SiC_4 grains.

Keywords: Al_4SiC_4; carbothermic reduction; hexagonal plate-like; growth mechanism

1 Introduction

Silicon-based non-oxide ceramic materials such as SiC and Si_3N_4 are widely used for high temperature applications due to their excellent high temperature properties. Exposing those silicon contained ceramics to oxygen containing atmosphere at high temperature leads to formation of a protective SiO_2 oxidation scale which can sufficiently prevent the further oxidation inwards [1,2]. However, the formed SiO_2 protective scale will be degraded significantly under certain atmospheric vapors as alkali vapor and/or water vapor due to the formation of volatile $Si(OH)_4$ phase [3]. For example, the oxidation kinetics of SiC ceramics increased with enhanced water vapor content and the oxidation rates were approximately one order of magnitude higher than the one observed in the dry oxygen in the 1200–1400 ℃ temperature range [4]. Thus the application of the silicon-based non-oxide ceramic materials under severe conditions is challenged.

Ternary carbide Al_4SiC_4 has received extensive attention because of its salient properties such as high melting point (≈ 2080 ℃), low density (3.03 g/cm^3), relative high toughness (3.98±0.05 MPa·m$^{1/2}$), high compressive strength (260 GPa) as well as remarkable

* Corresponding authors.
E-mail: J. Chen, cjh2666@126.com;
X. Hou, houxinmeiustb@ustb.edu.cn

resistance to oxidation and hydration at high temperature [5–9]. It is worth noting that under high temperature oxidation condition, a dual protective layer consisting of inner mullite and outer alumina is formed on the Al_4SiC_4 surface which can improve the oxidation resistance even in water vapor atmosphere [5,9,10]. However, the application of Al_4SiC_4 is confined due to the difficulty in fabricating highly pure samples. Hence, most of reported research work focused on the synthesis of this ternary ceramic. There are mainly three kinds of powder mixtures used to synthesize the Al_4SiC_4 powders or bulk, i.e., (1) using aluminum, silicon, and carbon powders as raw materials [11–13], (2) using Al_4C_3 and SiC powders as raw materials [14,15], and (3) using Al_2O_3, SiO_2, and C as raw materials by carbothermic reduction [16–20]. The former two reactant mixtures require expensive and active metal powders or carbides as starting materials. In addition, Al_4C_3 powders are also very easy to hydrate which often leads to sample pulverization [21]. In recent years, carbothermic reduction has become a promising synthesis route for high temperature ceramics because of its low requirements on starting materials. Both industrial raw materials such as commercial alumina and quartz and natural minerals such as sintered bauxite and kaolin can be adopted as starting materials, leading to great industrialization potential [19,20,22–25]. Some attempts have been done to synthesize highly pure Al_4SiC_4 by carbothermic reduction [17]. Furthermore, it has been found that the synthesized Al_4SiC_4 powders through carbothermic reduction usually have plate-like grains [16,17]. For the reaction mechanism, Lee *et al.* [17,18] reported that gas–solid reactions occur in the initial stage and gas–gas reactions in the latter stage by carbothermic reduction by using $Al(OH)_3$, SiO_2, and phenolic resin as starting materials. However, Yu *et al.* [20] argued that some solid–liquid reactions also occur as well during the synthesis and proposed that the metal phases such as Al and Si with low melting points are formed and wrap the Al_4SiC_4 particles, which accelerate the nucleation of Al_4SiC_4 grains. Hence, the reaction mechanism for synthesis of Al_4SiC_4 is still unclear. Furthermore, the gas phase formation during carbothermic reduction may play important roles in grain growth of Al_4SiC_4. However, limited work has been done to investigate the microstructural evolution of Al_4SiC_4 phase during the synthesis process by carbothermic reduction.

In the present work, highly pure Al_4SiC_4 powders were prepared by carbothermic reduction. The reaction mechanism was proposed in combination of experimental results and the thermodynamic calculation. Based on the microstructure analysis, the growth mechanism of the hexagonal plate-like Al_4SiC_4 grains was further evaluated using first-principles calculation.

2 Experimental details

Powders of analytically pure alumina (α-Al_2O_3 > 98.1%, average grain size: 10 μm), analytically pure silica (quartz > 98.8%, average grain size: 25 μm), and graphite (carbon content > 99.0%, average grain size: 30 μm) were purchased from Sinopharm Chemical Reagent Co., Ltd., Beijing, China, and adopted as raw materials. The raw materials were mixed according to the stoichiometric mole ratio of Al_2O_3:SiO_2:C = 2:1:12 (the ratio is based on the overall reaction: $2Al_2O_3+SiO_2+12C=Al_4SiC_4+8CO$) and ball milled for 24 h on a planetary ball mill with alumina grinding-balls using ethanol as the dispersive medium. This process is in favor of the uniform mix of the raw materials. Then the mixture was dried and cold compacted into a cylinder with 25 mm in diameter under a pressure of 30 MPa. The cylinder samples were placed into a graphite crucible with a cover and calcined at 2173 K for 8 h with a heating rate of 10 K/min in a graphite electric furnace. The furnace was vacuumed in advance and then highly pure Ar gas (purity ≥ 99.995%) was introduced into the furnace at the flow rate of 0.2 L/min. Finally, the furnace was cooled naturally to room temperature and the yellow product was obtained.

The phases were identified by X-ray diffraction (XRD; D8 Advance, Bruker, Germany). The morphology and composition of the product were examined by scanning electron microscopy (SEM; Nova Nano 450, FEI, USA) with energy dispersive spectrometer (EDS; TEAM, EDAX, USA). The structure was further characterized using transmission electron microscopy (TEM; JEM-2010, JEC, Japan) with the selected area electron diffraction (SAED).

The surface energy of Al_4SiC_4 grains at (0010) and $(1\bar{1}0)$ planes was calculated by first-principles calculation (FPC) based on the density functional theory (DFT). Firstly, the unit cell of Al_4SiC_4 and the slab models of the crystal planes with a space layer thickness of 15 Å were established by Materials Studio

7.0 software. Then the surface energy of the crystal was calculated by Cambridge Serial Total Energy Package module (CASTEP) [26]. For the calculation, the ultrasoft pseudopotential based on general gradient approximation (GGA) was adopted [27]. The cut-off energy of the plane wave (E_{cut}) was 450 eV. The sampling k-point mesh in the first irreducible Brillouin zone was generated by Monkhorst–Pack method, using a 6×6×1 grid for each structure. The convergence accuracy of the iteration was 5×10^{-6} per atom. The whole energy calculation was conducted in the reciprocal space.

3 Results and discussion

3. 1 Phase and microstructure characterization

The XRD pattern of the obtained product via carbothermic reduction of $Al_2O_3/SiO_2/C$ powder mixture at 2173 K for 8 h is shown in Fig. 1. Most of the diffraction peaks is consistent with the standard card of Al_4SiC_4 (PDF No. 35-1072) and the relative X-ray intensity ratio of the (0010) and $(1\bar{1}0)$ planes ($I_{(0010)}/I_{(1\bar{1}0)}$) of Al_4SiC_4 is much higher than the standard PDF card, indicating a preferential grain growth orientation [28]. In addition, the presence of a small amount of 4H-SiC and carbon in the final product may be due to the intermediate phase formation during the carbothermic reduction process and residual carbon powders from the raw materials, respectively.

The SEM images of the synthesized product shown in Fig. 2 are characterized as the plate-like grains. The

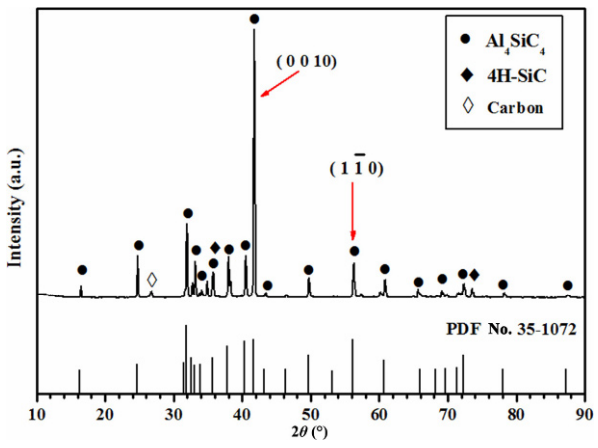

Fig. 1 XRD analysis of the product obtained by carbothermic reduction of $Al_2O_3/SiO_2/C$ powder mixture at 2173 K for 8 h.

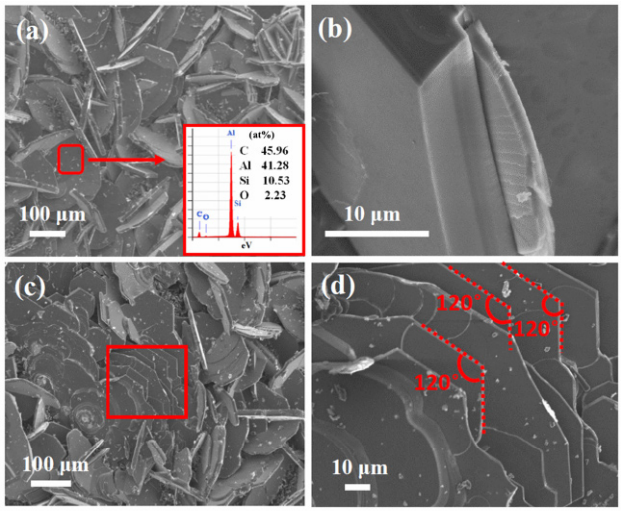

Fig. 2 SEM images of the synthesized Al_4SiC_4 powders by carbothermic reduction. (a) General morphology of synthesized Al_4SiC_4 powders, the inset: EDS analysis of the grain in the rectangle in (a); (b) thickness of the grains; (c) and (d) detailed stacking layer of Al_4SiC_4 grains with hexagonal plate-like feature; (d) enlarged SEM image of the red rectangle in (c).

EDS analysis in the bottom right corner of Fig. 2(a) shows that the atom ratio of Al:Si:C is close to 4:1:4, which further confirms the formation of the Al_4SiC_4 phase. The diameter of the Al_4SiC_4 grains ranges in 200–300 μm while the thickness is in the 2–6 μm range, as shown in Figs. 2(a) and 2(b). The typical stack-layer morphology of synthesized Al_4SiC_4 shown in Figs. 2(c) and 2(d) demonstrates clear hexagonal plate-like feature with an edge angle of approximately 120°.

Figure 3(a) shows a TEM image of one Al_4SiC_4 particle and the corresponding SAED pattern pattern is shown in Fig. 3(b). The SAED pattern was obtained by tilting the specimen into the respective zone axis (ZA) in independent alignment experiments. The SAED pattern in Fig. 3(b) is valid for the [0010] ZA of hexagonal Al_4SiC_4 (ICSD-606255). It indicates that the larger top surface is corresponding to the (0010) facet

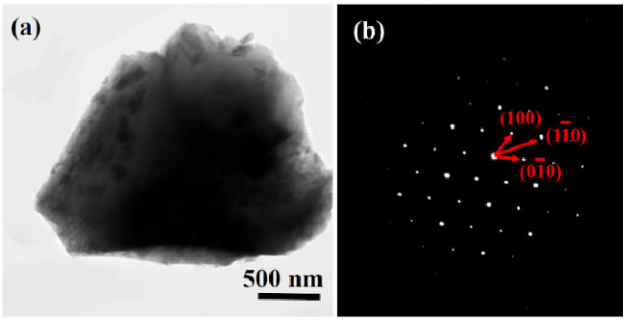

Fig. 3 (a) TEM image and (b) SAED pattern in the transparent part near edge of the Al_4SiC_4 particle.

and the one perpendicular the top surface is corresponding to $(1\bar{1}0)$ facet [29]. Since the Al_4SiC_4 grains grew into hexagonal plate eventually, it is proposed that the grown rate of plane (0010) is slower than the one of plane $(1\bar{1}0)$ during the carbothermic reduction process.

For the grain morphology, the Al_4SiC_4 grains with several kinds of morphologies are found in the crucible, which may mean the different growth mechanisms of Al_4SiC_4 during the growth process (see Fig. 4). Figure 4(a) shows the morphology of Al_4SiC_4 grain which has a smooth edge. Several shallow growing striations are clearly present on the surface of the grain. With the growth proceeding, grain growth along the $(1\bar{1}0)$ plane became dominated showing a step-like growth (Fig. 4(b)). The height of each stacked grain is about 2 μm as shown in the inset of Fig. 4(b). Eventually, the development of grain becomes complete because of the presence of straight grain edges and the sharp grain corners (Fig. 4(c)) which exist as the dominant morphology of Al_4SiC_4 in the final product. Only when the edge of the original Al_4SiC_4 grain becomes thicker, the more reactant gases will deposit on the lateral $(1\bar{1}0)$ plane. Then the edge of the grain will present the hexagonal crystal growth habit, which makes the edge change from smooth to straight. Such kind grain evolution will be further discussed using 2D nucleation and growth mechanism in the later part.

3. 2 Reaction mechanism

It should be pointed out that some golden isolated plate-like grains were observed on the cover and wall of the crucible after the calcination of the powder mixture at 2173 K for 8 h. Those grains were much larger than the internal grains. This may be attributed to the grain development derived from the solid–gas reactions or gas–gas reactions during the grain growth [30]. Hence the gas phase formation during the carbothermic reduction process was determined by thermodynamic calculation.

Concerning the thermodynamic calculation, systems of Si–O–C and Al–O–C are applied for the present study, which are considered as the possible reactions involving the synthesis of Al_4SiC_4 phase by carbothermic reduction. In the Si–O–C system, the possible solid phases are SiC and SiO_2. The reaction between SiO_2 and C is following [16]:

$$SiO_2(s)+3C(s)=SiC(s)+2CO(g) \quad (1)$$

$$\Delta_r G(P,T)=589314-328T+8.314\cdot\ln 10\cdot T\cdot 2\log(P_{CO(g)}/P^{\theta})(J\cdot mol^{-1})$$

Equation (1) can reach thermodynamic equilibrium at the experimental temperature (2173 K) by adjusting the CO(g) partial pressure, i.e., $\Delta_r G(P,T)=0$. Thus, the relationship between the reaction equilibrium constant of Eq. (1) and the CO(g) partial pressure at 2173 K can be calculated as following:

$$\log K_{2173K}=(-589114+328\times 2173)/(19.14\times 2173)=2\log(P_{CO(g)}/P^{\theta})=2.97$$

In the Si–O–C system, the possible gases are Si(g), Si_2(g), Si_3(g), SiO(g), SiO_2(g), and Si_2C(g). The related reactions and constants are listed in Table 1.

For the Al–O–C system, the possible solid phases are Al_2O_3, Al_4O_4C, and Al_4C_3. The reaction between Al_2O_3 and C is following [16–18]:

$$2Al_2O_3(s)+3C(s)=Al_4O_4C(s)+2CO(g) \quad (2)$$

$$\Delta_r G(P,T)=779220-348T+8.314\cdot\ln 10\cdot T\cdot 2\log(P_{CO(g)}/P^{\theta})(J\cdot mol^{-1})$$

$$\log K_{2173K}=(-779220+348\times 2173)/(19.14\times 2173)=\log(P_{CO(g)}/P^{\theta})=-0.55$$

Similarly, the reaction between Al_4O_4C and C is following:

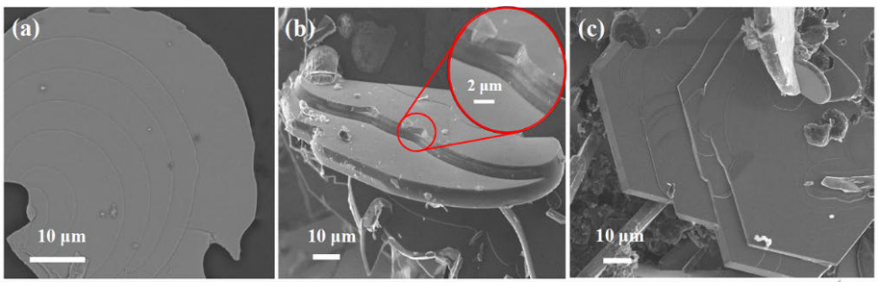

Fig. 4 SEM images of synthesized Al_4SiC_4 grains with different morphologies. (a) Grain with shallow smooth edges and striations; (b) grain with thick smooth edges and striations; (c) the well-developed grain with straight edges and sharp corners.

Table 1 Reactions and related thermodynamic data in the Si–O–C system at 2173 K

Equation	Reaction constant at 2173 K
$SiC(s)=Si(g)+C(s)$	$\log(P_{Si(g)}/P^{\theta})=-4.48$
$2SiC(s)=Si_2(g)+2C(s)$	$\log(P_{Si_2(g)}/P^{\theta})=-7.37$
$3SiC(s)=Si_3(g)+2C(s)$	$\log(P_{Si_2(g)}/P^{\theta})=-8.99$
$SiC(s)+CO(g)=SiO(g)+2C(s)$	$\log(P_{SiO(g)}/P^{\theta})-\log(P_{CO(g)}/P^{\theta})=-1.85$
$SiC(s)+2CO(g)=SiO_2(g)+3C(s)$	$\log(P_{SiO_2(g)}/P^{\theta})-2\log(P_{CO(g)}/P^{\theta})=-8.37$
$2SiC(s)=Si_2C(g)+C(s)$	$\log(P_{Si_2C(g)}/P^{\theta})=-7.37$
$SiO_2(s)+2C(s)=Si(g)+2CO(g)$	$\log(P_{Si(g)}/P^{\theta})+2\log(P_{CO(g)}/P^{\theta})=-1.53$
$2SiO_2(s)+4C(s)=Si_2(g)+4CO(g)$	$\log(P_{Si_2(g)}/P^{\theta})+4\log(P_{CO(g)}/P^{\theta})=-1.46$
$3SiO_2(s)+6C(s)=Si_3(g)+6CO(g)$	$\log(P_{Si_3(g)}/P^{\theta})+6\log(P_{CO(g)}/P^{\theta})=-0.12$
$SiO_2(s)+C(s)=SiO(g)+CO(g)$	$\log(P_{SiO(g)}/P^{\theta})+\log(P_{CO(g)}/P^{\theta})=1.11$
$SiO_2(s)=SiO_2(g)$	$\log(P_{SiO_2(g)}/P^{\theta})=-5.41$
$2SiO_2(s)+5C(s)=Si_2C(g)+4CO(g)$	$\log(P_{Si_2C(g)}/P^{\theta})+4\log(P_{CO(g)}/P^{\theta})=0.08$

$$Al_4O_4C(s)+6C(s)=Al_4C_3(s)+4CO(g) \quad (3)$$

$$\Delta_r G(P,T)=1568670-688T+8.314\cdot\ln 10\cdot T \cdot 4\log(P_{CO(g)}/P^{\theta})(J\cdot mol^{-1})$$

$$\log K_{2173K}=(-1568670+688\times 2173)/(19.14\times 2173)=\log(P_{CO(g)}/P^{\theta})=-1.77$$

In the Al–O–C system, the possible gases are Al(g), $Al_2O(g)$, AlO(g), and $Al_2O_2(g)$. The related reactions and constants are listed in Table 2.

Figure 5 shows the equilibrium partial pressures of all gases formed in the Al–Si–C–O system at 2173 K determined by thermodynamic calculation using FactSage 7.0 thermodynamic calculation software. At this temperature, the gas phases of SiO(g), Al(g), and $Al_2O(g)$ have relatively high partial pressures and were considered as the main reactant gases during the carbothermic reduction process.

For the reduction of SiO_2 phase, it will be reduced firstly and large amount of SiO(g) can be generated during this process. At the same time, the generated SiO(g) can immediately react with carbon and CO(g) to form SiC according to the following reactions [17,18]:

$$SiO(g)+2C(s)=SiC(s)+CO(g) \quad (4)$$

$$SiO(g)+3CO(g)=SiC(s)+3CO_2(g) \quad (5)$$

However, when SiC solid phase is formed on the graphite, Eq. (4) will be hindered or become slow because the diffusion rate of the solid carbon and SiO(g) is reduced significantly due to the new formed SiC solid phase. Then, the reaction in Eq. (5) becomes dominated for the further producing of SiC phase. Therefore, the possible reaction route for synthesis of SiC can be ascribed to a gas–solid reaction and a gas–gas reaction.

Concerning the reduction of Al_2O_3 phase, it was considered as the main source of the Al_4C_3 and Al-containing intermediate phase. However, another intermediate phase (Al_4O_4C) is also observed during the conversion of Al_2O_3 into Al_4C_3 phase (Fig. 5). During the reduction reaction of Al_4O_4C, a large amount of Al(g) and $Al_2O(g)$ will be generated [31,32]. These Al-containing gases can react with carbon to form Al_4C_3 as follows:

Table 2 Reactions and related thermodynamic data in the Al–O–C system at 2173 K

Equation	Reaction constant at 2173 K
$Al_4C_3(s)=4Al(g)+3C(s)$	$4\log(P_{Al(g)}/P^{\theta})=-7.62$
$Al_4C_3(s)+2CO(g)=2Al_2O(g)+5C(s)$	$2\log(P_{Al_2O(g)}/P^{\theta})-2\log(P_{CO(g)}/P^{\theta})=-2.14$
$Al_4C_3(s)+4CO(g)=4AlO(g)+7C(s)$	$4\log(P_{AlO(g)}/P^{\theta})-4\log(P_{CO(g)}/P^{\theta})=-21.88$
$Al_4C_3(s)+4CO(g)=2Al_2O_2(g)+7C(s)$	$2\log(P_{Al_2O_2(g)}/P^{\theta})-4\log(P_{CO(g)}/P^{\theta})=-10.64$
$Al_2O_3(s)+3C(s)=2Al(g)+3CO(g)$	$2\log(P_{Al(g)}/P^{\theta})+3\log(P_{CO(g)}/P^{\theta})=-5.04$
$Al_2O_3(s)+2C(s)=Al_2O(g)+2CO(g)$	$\log(P_{Al_2O(g)}/P^{\theta})+2\log(P_{CO(g)}/P^{\theta})=-2.30$
$Al_2O_3(s)+C(s)=2AlO(g)+CO(g)$	$2\log(P_{AlO(g)}/P^{\theta})+\log(P_{CO(g)}/P^{\theta})=-12.17$
$Al_2O_3(s)+C(s)=Al_2O_2(g)+CO(g)$	$\log(P_{Al_2O_2(g)}/P^{\theta})+\log(P_{CO(g)}/P^{\theta})=-6.55$
$Al_4O_4C(s)+3C(s)=4Al(g)+4CO(g)$	$4\log(P_{Al(g)}/P^{\theta})+4\log(P_{CO(g)}/P^{\theta})=-9.52$
$Al_4O_4C(s)+C(s)=2Al_2O(g)+2CO(g)$	$2\log(P_{Al_2O(g)}/P^{\theta})+2\log(P_{CO(g)}/P^{\theta})=-4.04$
$Al_4O_4C(s)=4AlO(g)+C(s)$	$4\log(P_{AlO(g)}/P^{\theta})=-23.79$
$Al_4O_4C(s)=2Al_2O_2(g)+C(s)$	$2\log(P_{Al_2O_2(g)}/P^{\theta})=-12.55$

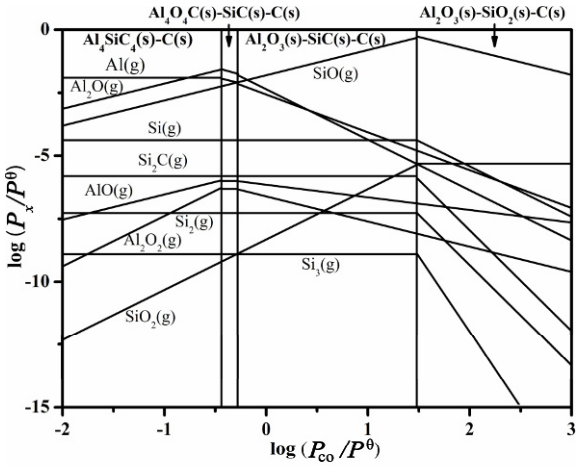

Fig. 5 Equilibrium partial pressures of gases formed in the Al–Si–C–O system.

$$4Al(g)+3C(s)=Al_4C_3(s) \quad (6)$$

$$2Al_2O(g)+5C(s)=Al_4C_3(s)+2CO(g) \quad (7)$$

According to the previous study [33], the Al_4SiC_4 can be formed by the solid reaction between SiC and Al_4C_3 (Eq. (8)):

$$Al_4C_3(s)+SiC(s)=Al_4SiC_4(s) \quad (8)$$

In addition to the reaction in Eq. (8), Al_4SiC_4 may also be precipitated by the gas–gas reactions between Si and Al contained gas phases such as SiO(g), Al(g), and Al_2O(g), etc. Although SiO_2 has been reduced into SiC phase, the gas phases of SiO(g) and Al_2O(g) may also be generated through Eq. (9) [34]:

$$Al_2O_3(s)+SiC(s)=Al_2O(g)+SiO(g)+CO(g) \quad (9)$$

Because of the relative high heating rate, the main reactant gases can participate in the following gas–solid reactions (Eqs. (10) and (11)) for the formation of Al_4SiC_4 during the reducing reaction:

$$4Al(g)+SiO(g)+5C(s)=Al_4SiC_4(s)+CO(g) \quad (10)$$

$$2Al_2O(g)+SiO(g)+7C(s)=Al_4SiC_4(s)+3CO(g) \quad (11)$$

However, Eqs. (10) and (11) may only occur at the initial stage to form Al_4SiC_4 nucleus since the reaction rate will be decreased quickly because of the presence of solid Al_4SiC_4 covering on the carbon surface. Therefore, another possible reaction route for the formation of Al_4SiC_4 during the carbothermic reduction can be subjected to following gas–gas reactions (Eqs. (12) and (13)):

$$4Al(g)+SiO(g)+9CO(g)=Al_4SiC_4(s)+5CO_2(g) \quad (12)$$

$$2Al_2O(g)+SiO(g)+11CO(g)=Al_4SiC_4(s)+7CO_2(g) \quad (13)$$

Hence, based on the thermodynamic calculation in the Al–Si–O–C system, the formation of Al_4SiC_4 during the carbothermic reduction process was not confined to the solid–solid reaction but also from the gas–solid reactions and gas–gas reactions where some Al and Si containing intermediate gases such as Al(g), Al_2O(g), and SiO(g) were involved in the reaction process.

3.3 Grain growth mechanism

As shown in Fig. 6, Al_4SiC_4 owns a $P6_3mc$ space group and a hexagonal crystal structure which can be described as layered structure stacked with the 4H-SiC type units and Al_4C_3 type units alternative along the *c*-axis [35,36]. It has been reported that the development of the hexagonal grains depends on the grain growing rate of (0010) and $(1\bar{1}0)$ planes which is closely related to the surface energy. Thus, the surface energy of (0010) and $(1\bar{1}0)$ planes can be calculated by FPC using Eq. (14) based on DFT [37,38]:

$$E_{surf}=\frac{E_{slab}-nE_{bulk}}{A} \quad (14)$$

Here, E_{surf} is the surface energy, E_{slab} is the total energy of the slab per unit cell, E_{bulk} is the energy per atom in an infinite crystal, n is the number of atoms in the slab unit cell, and A is the specific surface area of the slab unit cell.

The obtained surface energy along plane (0010) and plane $(1\bar{1}0)$ by FPC (Table 3) indicates that plane (0010) of Al_4SiC_4 possesses much higher surface energy which is almost two times that of plane $(1\bar{1}0)$. According to the Gibbs–Wulff theory, the plane with higher energy grows faster and eventually disappears

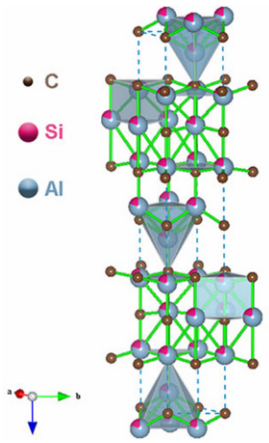

Fig. 6 Crystal structure of Al_4SiC_4.

Table 3 Surface energy of different planes

Crystal plane	(0010)	$(1\bar{1}0)$
Surface energy (J/m^2)	1.07	0.58

during growth [39]. Then the low surface energy plane will compose the main surface of the crystal. Based on this mechanism, a hexagonal prismatic Al_4SiC_4 shall be obtained. However, the obtained Al_4SiC_4 crystals in our work are more plate-like shape instead of hexagonal prismatic shape.

Therefore the growth of plate-like Al_4SiC_4 grain might be controlled by two-dimensional (2D) nucleation and growth mechanism [40]. The 2D nucleation and growth includes two different steps: one is the discontinuous 2D nucleation and the other is the continuous side expansion of the planes. The growth schematic diagram of plate-like Al_4SiC_4 grain is illustrated in Fig. 7. In the beginning, the original graphite and some solid carbides formed through the solid–solid reactions or solid–gas reactions are worked as the substrates where the reactant gases such as SiO(g), Al(g), and Al_2O(g) generated in this system can be absorbed on it. At the atom sites where the 2D nucleation barrier is low, some generated gas molecules can form short lived unions and have the chance to form embryos with the size equal to or larger than the critical nucleus size. These embryos then become the nucleus of the 2D growth of Al_4SiC_4. Subsequently the reactant gases continue to collide and be absorbed on the surface. When diffusing on the perfect area of the surface, the absorbed gases have weak combination with surface and exist extra broken bonds. Only at the kink or step sites, the gases can form stable bonds with surface atom, become more stable and favor the lateral growth and spreading. Once one layer of flat grain surface is achieved, a new grain nucleus will be formed on the incomplete layers as well as at old flat grain surface [41]. And such a kind of reactions between the substrates and gases will occur repeatedly during the carbonthermic reduction. Hence, the growth of the Al_4SiC_4 grain is not continuous which also explains the growth striations and the stacking layer-by-layer structure formation shown in Fig. 4.

According previous studies [42,43], for the two-dimensional nucleation and growth of the hexagonal plate-like microstructure, a high gas supersaturation that reaches the requirement of $(p/p_c)_{crit}$ of both the high-energy planes and the low-energy planes is required. Since large amounts of gas phases such as SiO(g), Al(g), and Al_2O(g) can be generated during the carbothermic reduction process in this work, they could ensure sufficient gas supersaturation in this system that required for 2D nucleation and growth of both the high-energy plane (0010) and the low-energy plane $(1\bar{1}0)$. The high supersaturation vapor pressure will ensure enough gases attached on plane $(1\bar{1}0)$ which favors the 2D nucleation and growth of the low-energy plane while the growth at high-energy plane (0010) has already been completed leading to formation of plate-like Al_4SiC_4 grains as shown in Figs. 4(b) and 4(c).

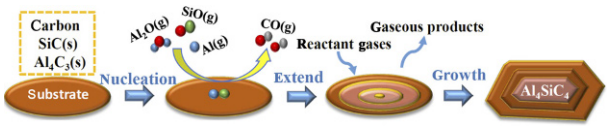

Fig. 7 Schematic illustration of two-dimensional nucleation and growth of Al_4SiC_4 grain.

4 Conclusions

Al_4SiC_4 powders with hexagonal plate-like morphology were successfully prepared through carbothermic reduction. Based on the product morphology and grain surface growth characteristics, it is deduced that such gases as SiO(g), Al(g), Al_2O(g), and CO(g) are crucial intermediates during the synthesis process. For the grain development, it follows the two-dimensional nucleation and growth theory which is closely related to the surface energy and gas supersaturation partial pressure.

Acknowledgements

The authors express their appreciation to the National Science Fund for Excellent Young Scholars of China (No. 51522402). The authors also appreciate the National Natural Science Foundation of China (Nos. 51572019 and U1460201) and the Central Universities of FRF-TP-15-006C1 for financial support.

References

[1] Liu D-M. Oxidation of polycrystalline α-silicon carbide ceramic. *Ceram Int* 1997, **23**: 425–436.
[2] Shimada S, Aketo T. High-temperature oxidation at 1500 ℃ and 1600 ℃ of SiC/graphite coated with sol–gel-derived HfO_2. *J Am Ceram Soc* 2005, **88**: 845–849.
[3] Pareek V, Shores DA. Oxidation of silicon carbide in environments containing potassium salt vapor. *J Am Ceram Soc* 1991, **74**: 556–563.
[4] Opila EJ. Variation of the oxidation rate of silicon carbide with water-vapor pressure. *J Am Ceram Soc* 1999, **82**: 625–636.
[5] Wills R, Goodrich S. The oxidation of aluminum silicon

carbide. In: Proceedings of the 29th International Conference on Advanced Ceramics and Composites, 2009, **322**: 181–188.
[6] Viala JC, Fortier P, Bouix J. Stable and metastable phase equilibria in the chemical interaction between aluminium and silicon carbide. *J Mater Sci* 1990, **25**: 1842–1850.
[7] Wen GW, Huang XX. Increased high temperature strength and oxidation resistance of Al_4SiC_4 ceramics. *J Eur Ceram Soc* 2006, **26**: 1281–1286.
[8] Itatani K, Takahashi F, Aizawa M, *et al.* Densification and microstructural developments during the sintering of aluminium silicon carbide. *J Mater Sci* 2002, **37**: 335–342.
[9] Yamaguchi A, Zhang S. Synthesis and some properties of Al_4SiC_4. *J Ceram Soc Jpn* 1995, **103**: 20–24.
[10] Huang XX, Wen GW, Cheng XM, *et al*. Oxidation behavior of Al_4SiC_4 ceramic up to 1700 ℃. *Corros Sci* 2007, **49**: 2059–2070.
[11] Chen JH, Zhang ZH, Mi WJ, *et al.* Fabrication and oxidation behavior of Al_4SiC_4 powders. *J Am Ceram Soc* 2017, **100**: 3145–3154.
[12] Lee SH, Oh HC, An BH, *et al*. Ultra-low temperature synthesis of Al_4SiC_4 powder using spark plasma sintering. *Scripta Mater* 2013, **69**: 135–138.
[13] Yao H, Xing X, Wang E, *et al.* Oxidation behavior and mechanism of Al_4SiC_4 in MgO–C–Al_4SiC_4 system. *Coatings* 2017, **7**: 85.
[14] Oscroft RJ, Thompson DP. Influence of oxygen on the formation of aluminum silicon carbide. *J Am Ceram Soc* 2005, **75**: 224–226.
[15] Hasegawa M, Itatani K, Aizawa M, *et al*. Low-temperature synthesis of aluminum silicon carbide using ultrafine aluminum carbide and silicon carbide powders. *J Am Ceram Soc* 1996, **79**: 275–278.
[16] Zhao J, Lin W, Yamaguchi A, *et al.* Synthesis of Al_4SiC_4 from alumina, silica and graphite. *J Ceram Soc Jpn* 2007, **115**: 761–766.
[17] Lee J-S, Lee S-H, Nishimura T, *et al*. Hexagonal plate-like ternary carbide particulates synthesized by a carbothermal reduction process: Processing parameters and synthesis mechanism. *J Am Ceram Soc* 2009, **92**: 1030–1035.
[18] Lee J-S, Lee S-H, Nishimura T, *et al*. Synthesis of mono-phase, hexagonal plate-like Al_4SiC_4 powder via a carbothermal reduction process. *J Ceram Soc Jpn* 2008, **116**: 717–721.
[19] Yu C, Zhu H, Yuan W, *et al*. Synthesis and oxidation behavior of Al_4SiC_4–Al–Si composites. *Int J Mater Res* 2014, **105**: 793–796.
[20] Yu C, Yuan W, Deng C, *et al*. Synthesis of hexagonal plate-like Al_4SiC_4 from calcined bauxite, silica and carbon black. *Powder Technol* 2013, **247**: 76–80.
[21] Yu J, Yamaguchi A. Hydration of synthesized Al_4C_3 and its prevention effect by Si addition. *J Ceram Soc Jpn* 1995, **103**: 475–478.
[22] Yuan WJ, Li J, Pan C. Synthesis of Al_4SiC_4 powders from kaolin grog, aluminum and activated carbon as raw materials. *Adv Mater Res* 2012, **399–401**: 788–791.
[23] Shi Z, Fan R, Yan K, *et al*. Preparation of iron networks hosted in porous alumina with tunable negative permittivity and permeability. *Adv Funct Mater* 2013, **23**: 4123–4132.
[24] Cheng C, Yan K, Fan R, *et al*. Negative permittivity behavior in the carbon/silicon nitride composites prepared by impregnation-carbonization approach. *Carbon* 2016, **96**: 678–684.
[25] Shi Z, Fan R, Zhang Z, *et al*. Random composites of nickel networks supported by porous alumina toward double negative materials. *Adv Mater* 2012, **24**: 2349–2352.
[26] Segall MD, Lindan P, Probert MJ, *et al*. First-principles simulation: Ideas, illustrations and the CASTEP code. *J Phys: Condens Matter* 2002, **14**: 2717–2744.
[27] Vanderbilt D. Soft self-consistent pseudopotentials in a generalized eigenvalue formalism. *Phys Rev B* 1990, **41**: 7892–7895.
[28] Sakka Y, Suzuki T. Textured development of feeble magnetic ceramics by colloidal processing under high magneticfield. *J Ceram Soc Jpn* 2005, **113**: 26–36.
[29] Du W, Deng D, Han Z, *et al*. Hexagonal tin disulfide nanoplatelets: A new photocatalyst driven by solar light. *CrystEngComm* 2011, **13**: 2071–2076.
[30] Jung C-H, Lee M-J, Kim C-J. Preparation of carbon-free B_4C powder from B_2O_3 oxide by carbothermal reduction process. *Mater Lett* 2004, **58**: 609–614.
[31] Lefort P, Tetard D, Tristant P. Formation of aluminum carbide by carbothermal reduction of alumina: Role of the gaseous aluminum phase. *J Eur Ceram Soc* 1993, **12**: 123–129.
[32] Fruehan RJ, Li Y, Carkin G. Mechanism and rate of reaction of Al_2O, Al, and CO vapors with carbon. *Metall Mater Trans B* 2004, **35**: 617–623.
[33] Oden LL, Mccune RA. Phase equilibria in the Al–Si–C system. *Metall Mater Trans A* 1987, **18**: 2005–2014.
[34] Gadalla A. High temperature reactions within SiC–Al_2O_3 composites. *J Mater Res* 1992, **7**: 2585–2592.
[35] Pedesseau L, Even J, Modreanu M, *et al*. Al_4SiC_4 wurtzite crystal: Structural, optoelectronic, elastic, and piezoelectric properties. *APL Mater* 2015, **3**: 121101–121108.
[36] Liao T, Wang J, Zhou Y. Atomistic deformation modes and intrinsic brittleness of Al_4SiC_4: A first-principles investigation. *Phys Rev B* 2006, **74**: 174112.
[37] Casassa S, Pisani C. Atomic-hydrogen interaction with metallic lithium: An *ab initio* embedded-cluster study. *Phys Rev B* 1995, **51**: 7805–7816.
[38] Polatoglou HM, Methfessel M, Scheffler M. Vacancy-formation energies at the (111) surface and in bulk Al, Cu, Ag, and Rh. *Phys Rev B* 1993, **48**: 1877–1883.
[39] Lazzeri M, Vittadini A, Selloni A. Structure and energetics of stoichiometric TiO_2 anatase surfaces. *Phys Rev B* 2001, **63**: 155409
[40] Liu XY, Maiwa K, Tsukamoto K. Heterogeneous two-dimensional nucleation and growth kinetics. *J Chem Phys* 1997, **106**: 1870–1879.
[41] Nielsen AE. *International Series of Monographs on Analytical Chemistry*. New York: Pergamon, 1964.
[42] Lewis B. The growth of crystals of low supersaturation: I. Theory. *J Cryst Growth* 1974, **21**: 29–39.
[43] Lewis B. The growth of crystals at low supersaturation: II.

Comparison with experiment. *J Cryst Growth* 1974, **21**: 40–50.